Control of the metal–insulator transition in vanadium dioxide by modifying orbital occupancy

Nagaphani B. Aetukuri[1,2]★, Alexander X. Gray[3], Marc Drouard[1], Matteo Cossale[1], Li Gao[1], Alexander H. Reid[3], Roopali Kukreja[2,3], Hendrik Ohldag[4], Catherine A. Jenkins[5], Elke Arenholz[5], Kevin P. Roche[1], Hermann A. Dürr[3], Mahesh G. Samant[1] and Stuart S. P. Parkin[1]★

External control of the conductivity of correlated oxides is one of the most promising schemes for realizing energy-efficient electronic devices. Vanadium dioxide (VO_2), an archetypal correlated oxide compound, undergoes a temperature-driven metal–insulator transition near room temperature with a concomitant change in crystal symmetry. Here, we show that the metal–insulator transition temperature of thin $VO_2(001)$ films can be changed continuously from ∼285 to ∼345 K by varying the thickness of the RuO_2 buffer layer (resulting in different epitaxial strains). Using strain-, polarization- and temperature-dependent X-ray absorption spectroscopy, in combination with X-ray diffraction and electronic transport measurements, we demonstrate that the transition temperature and the structural distortion across the transition depend on the orbital occupancy in the metallic state. Our findings open up the possibility of controlling the conductivity in atomically thin VO_2 layers by manipulating the orbital occupancy by, for example, heterostructural engineering.

Transitions from itinerant to localized electronic behaviour are ubiquitous in condensed-matter systems[1]. These transitions, especially in systems with d-electrons, originate from a complex interplay of instabilities in the charge, spin, orbital and lattice degrees of freedom[2–7]. VO_2 is a $3d^1$ system and conventional electron-counting rules would suggest a metallic ground state due to a half-filled outer shell. However, VO_2 exhibits a metal–insulator transition (MIT) near room temperature ($T_{MIT} \sim 340$ K in bulk) with an accompanying structural phase transition[8]. The nature of the low-temperature insulating phase of VO_2 is one of the long-standing debates, with recent literature suggesting that this phase should be considered a Peierls–Mott insulator wherein electron–electron correlations and dimerization of V ions both contribute to the opening of an insulating gap[9–11]. On the other hand, despite being extensively studied, the role of the metallic phase of VO_2 in triggering this transition and the electronic property that sets the energy scale for the transition temperature, T_{MIT}, have not yet been fully understood and identified. Yet, a fundamental understanding of the metallic phase and its role in triggering the MIT is critical to engineering devices based on the MIT in VO_2 and related materials. In this study, we elucidate the role of orbital occupations in the metallic phase and the lattice changes across the transition in differently strained single-crystalline VO_2 thin films where T_{MIT} is varied in a well-controlled manner by over ∼60 K. We furthermore find that the insulating state's orbital occupation changes little with strain, thus underlining the importance of the metallic state's electronic properties in governing the energy scale of the metal–insulator transition.

The high-temperature metallic phase of VO_2 has a rutile crystal structure with $P4_2/mnm$ space symmetry[12]. In this structure, shown in Fig. 1a with three rutile VO_2 unit cells, vanadium ions (orange)

occupy the octahedral interstices formed by oxygen ions (blue). The oxygen octahedra at the body-centre and the corner of a rutile unit cell are related by a 90° rotation about the rutile c axis (c_R) and share a common vertex. The octahedra of adjacent unit cells along c_R share a common edge. Across the MIT, the V^{4+} ions move away from the octahedral-interstice centre by a combination of an anti-ferroelectric distortion along the rutile [110] and [1$\bar{1}$0] directions and a dimerization along the [001] direction resulting in the monoclinic phase with a lowered crystal symmetry of $P2_1/c$ (ref. 13). This transition and the relationship between the rutile and the monoclinic phases are shown in the figure (also see Supplementary Fig. S1). The octahedra in VO_2 are orthorhombically distorted, making it possible to differentiate the apical and equatorial V–O bonds, as shown in Fig. 1b.

The structural transition in VO_2 is accompanied by changes in the electronic band structure near the Fermi level (E_F) that can be qualitatively understood within a crystal-field model, first proposed in ref. 14, resulting from the octahedral environment and the associated hybridization of the O $2p$ orbitals with V $3d$ orbitals (p–d hybridization) that are involved in chemical bonding. The $3d$ electronic levels of the V ion are crystal-field split into a combination of low-energy t_{2g} states (Fig. 1b) and high-energy e_g^σ states, where σ represents the symmetry of the V–O bonds. The small orthorhombic component of the crystal field associated with the different equatorial and apical V–O distances further separates the t_{2g} orbitals into a single a_{1g} orbital and a doubly degenerate e_g^π combination with π-type V–O bonds. The e_g^π and the e_g^σ orbitals hybridize with the O $2p$ orbitals and form low-energy bonding combinations with predominantly O $2p$ character and high-energy anti-bonding combinations with predominantly V $3d$ character. The a_{1g} orbitals ($d_\parallel$) are directed parallel to the rutile c axis (c_R)

[1]IBM Almaden Research Center, 650 Harry Road, San Jose, California 95120, USA, [2]Department of Materials Science and Engineering, Stanford University, Stanford, California 94305, USA, [3]Stanford Institute for Materials and Energy Sciences, SLAC National Accelerator Laboratory, 2575 Sand Hill Road, Menlo Park, California 94025, USA, [4]Stanford Synchrotron Radiation Lightsource, SLAC National Accelerator Laboratory, 2575 Sand Hill Road, Menlo Park, California 94025, USA, [5]Advanced Light Source, Lawrence Berkeley National Laboratory, Berkeley, California 94720, USA. *e-mail: phani@alumni.stanford.edu; stuart.parkin@us.ibm.com
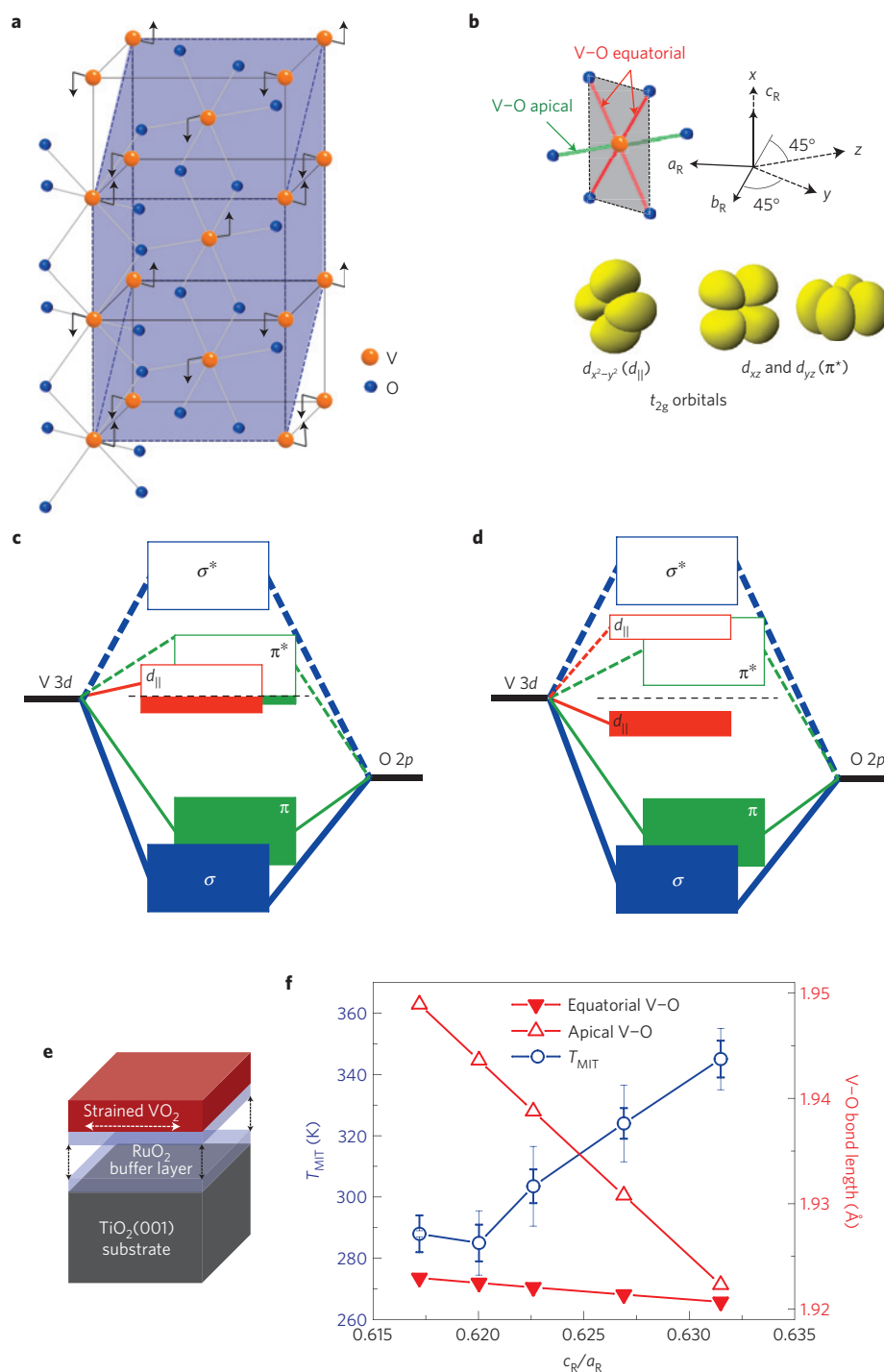
Figure 1 | Overview and strain-dependent MIT in VO₂. a, A schematic of the inter-relationship between the rutile (three adjacent units along the rutile c axis, c_R, are shown) and the monoclinic (shaded) crystal structures in VO_2. The oxygen octahedra at the body-center and the corners of the rutile unit cell are related by a 90° rotation about c_R. Across the MIT, the vanadium ions move away from the octahedral-site centre as shown by the black arrows. **b**, An octahedron at the centre of a rutile unit cell of VO_2 is redrawn to illustrate the orthorhombic distortion and the different apical and equatorial V–O bond lengths. The vanadium t_{2g} d orbitals that form the valence electronic states in VO_2 are shown along with the relationship between the rutile crystallographic axes (solid arrows) and the geometric axes of the orbitals (dashed arrows). **c,d**, Schematic of the VO_2 band structure in the metallic (**c**) and insulating (**d**) states. **e**, Schematic of strain transfer to the VO_2 thin films through a RuO_2 buffer layer of variable thickness deposited on a single-crystalline $TiO_2(001)$ substrate. **f**, Experimental data showing the continuous variation in T_{MIT} as a function of the axial ratio in the rutile phase (c_R/a_R). T_{MIT} is defined as the average of transition temperatures during cooling and warming. The thicker error bars represent the hysteresis in the resistance–temperature curves. The thinner error bars represent the width of the transition during cooling. The changes in the apical and the equatorial V–O bond lengths are also plotted.

and are relatively non-bonding with respect to O $2p$ (refs 14,15). In the metallic state, shown schematically in Fig. 1c, the density of states at E_F is formed from a mixture of the $d_{\parallel}$ orbitals that

are directed along c_R and the more isotropic and anti-bonding e_g^π orbitals (π^*). The π^* orbitals have a smaller p–d overlap in comparison with the e_g^σ orbitals (σ^*) and thus the latter are centred

at ~3.5 eV (ref. 16) above E_F. Across the MIT, the dimerization of the V ions along the c axis splits the highly directional $d_\parallel$ orbitals that mediate V–V bonds into a bonding and an anti-bonding combination. In addition to this, the anti-ferroelectric displacement perpendicular to c_R and parallel to the crystallographic $\langle 110 \rangle$ directions increases p–d overlap[13] and results in an energy upshift of the π^* orbitals. The net result, as shown in Fig. 1d, is orbital polarization[15,17] in the insulating state with bonding $d_\parallel$ orbitals being fully occupied and the anti-bonding $d_\parallel$ ($d_\parallel^*$) and π^* being empty. In this work, we induce systematic changes in the electronic structure near E_F by changing the p–d hybridization through lattice strain in thin films of VO_2.

We modify the strain in VO_2 thin films by depositing a buffer layer of ruthenium dioxide (RuO_2) between the film and the TiO_2 (001) substrate. RuO_2 is used because it has the same crystal structure and space group as both TiO_2 and metallic VO_2 ($P4_2/mnm$; refs 12,18,19). Furthermore, the lattice parameters of bulk RuO_2 ($a_{RuO_2} = 4.4910$ Å, $c_{RuO_2} = 3.1064$ Å) are such that the VO_2 (001) film (bulk $a_{VO_2} = 4.5546$ Å) is compressively strained in-plane when deposited on relaxed RuO_2 (001) whereas tensile-strained on TiO_2 (001) (bulk $a_{TiO_2} = 4.5937$ Å). This is shown schematically in Fig. 1e. Although the strain in VO_2 films can be changed by depositing VO_2 on differently oriented TiO_2 substrates[20], or by applying a uniaxial strain along [110] as has been done on VO_2 single crystals[21], such approaches change the structural symmetry of the metallic state of VO_2, making it difficult to distinguish between the effects of strain and/or symmetry. Our approach, in contrast, retains the tetragonal symmetry of the metallic state for all of the differently strained films and hence any accompanying electronic structure changes can be unambiguously attributed to changes in lattice parameters alone. Our work also identifies a way to continuously control the T_{MIT} in VO_2 thin films by epitaxial strain of a buffer layer of varying thickness.

VO_2 films were prepared by pulsed laser deposition on TiO_2 (001) substrates, with and without RuO_2 buffer layers. RuO_2 buffer layers of different thicknesses, namely ~10 nm, ~20 nm, ~40 nm and ~80 nm, were reactively sputtered (Methods). θ–2θ X-ray diffraction analysis of the films shows a continuous change in the out-of-plane lattice constant, c_R, of the VO_2 films as a function of increasing RuO_2 buffer layer thickness (Supplementary Fig. S3). In general, epitaxial strain in thin-film heterostructures is relieved by misfit dislocation formation[22]. Typically, as the thickness of the strained film is increased there will be a critical thickness below which the film is coherently strained and above which the strain will be partially relieved by the formation of increasing numbers of misfit dislocations, until eventually the film is completely relaxed. Our data indicate that the VO_2 films, each 30 nm thick, are coherently strained for each RuO_2 under-layer thickness, such that there is a monotonic decrease in the VO_2 (002) peak position with increasing RuO_2 thickness. On the other hand, the RuO_2 films themselves are rather incoherently strained such that the lower portion of the RuO_2 layer is clamped to the TiO_2 substrate and the upper portion of the film has a different lattice parameter owing to strain relaxation throughout the thickness of the RuO_2 film (Supplementary Fig. S2). As a consequence, the angular position of the diffraction peak from the VO_2 (002) planes decreases with increasing RuO_2 thickness (Supplementary Fig. S3), which is indicative of an increasing c_R. From the measured c_R, the in-plane lattice parameter of the VO_2 films, a_R, was calculated by assuming an isotropic biaxial stress induced in the VO_2 thin film (Supplementary Section S5). Temperature-dependent electrical transport measurements (Supplementary Figs S4 and S6) showed that the T_{MIT}, averaged over the warming and cooling curves that are different owing to the hysteretic transition, decreased by a maximum value of ~60 K for the maximally strained sample for which the axial ratio of the rutile phase, c_R/a_R, was decreased by

~2.3% (Fig. 1f and Supplementary Table S1). The decrease in c_R/a_R results in a significant increase in the apical V–O bond length, whereas the equatorial V–O bond length changes very little. These changes are also plotted in Fig. 1f.

On the basis of crystal-field arguments, we suggest that the increase in the apical V–O bond length decreases the p–d overlap and, consequently, decreases the energy level of the π^* orbitals relative to those of the $d_\parallel$ orbitals. This relative energy shift should then result in an increase of the orbital occupancy of the π^* orbitals and in a decrease of the occupancy of the $d_\parallel$ orbitals. Note that both the π^* and $d_\parallel$ orbitals are partially occupied at E_F in the metallic state. To test this hypothesis, we carried out polarization-dependent soft X-ray absorption spectroscopy measurements at the V $L_{2,3}$ edges for three VO_2 films with different transition temperatures to determine their orbital occupations in the insulating and in the metallic states[11]. These measurements were performed using total electron yield (TEY) detection[23]. Owing to the narrow bandwidth of the $3d$ valence electronic states and the relatively large valence-electron core–hole Coulomb interaction, the exciton created by the X-ray absorption process can be assumed to be strongly localized[9,24]. Thus, the X-ray absorption spectroscopy (XAS) data can be interpreted by means of dipole-allowed atomic-like transitions from the V $2p$ core level to the $3d$ valence electronic states, that is, a $2p^6 3d^1 \rightarrow 2p^5 3d^2$ transition. Linearly polarized X-rays with the electric-field orientation parallel ($\mathbf{E} \parallel c_R$) and perpendicular ($\mathbf{E} \perp c_R$) to the rutile c axis (Fig. 2a) probe the vacant $d_\parallel$ and π^* valence-electron states, respectively[11].

We first discuss the orbital occupation changes in the metallic and the insulating states for the sample with $T_{MIT} = $ ~345 K. In Fig. 2b, we plot the metallic-state polarization-dependent XAS spectra for this sample collected at 380 K. The main peaks in the spectra at ~518 eV and 524 eV, respectively, correspond to the V L_3 and L_2 absorption edges that originate from the $2p_{3/2} \rightarrow 3d$ and $2p_{1/2} \rightarrow 3d$ transitions[9]. XAS spectra collected with $\mathbf{E} \parallel c_R$ and $\mathbf{E} \perp c_R$ are similar, as expected from the isotropic orbital occupation in the metallic state, as shown in Fig. 1c, and demonstrated in previous experimental and theoretical studies[11,17]. However, there are subtle but notable differences between the two spectra that can be seen more readily in the dichroic signal that is also plotted in Fig. 2b. In contrast, in the insulating state the XAS spectra that were collected on the same sample at 270 K show a much larger dichroism (Fig. 2c), which is a clear signature of orbital polarization expected from the well-known V–V dimerization in the insulating state and the consequential selective filling of $d_\parallel$ orbitals[11,14]. The differences in the XAS spectra between the metallic and insulating states can be qualitatively understood from Fermi's golden rule by which the XAS intensity scales with the unoccupied density of states[17,25]. This means that $I_\parallel \propto \rho_{d_\parallel}$ and $I_\perp \propto \rho_{\pi^*}$, where $I_\parallel$ and $I_\perp$ are the XAS intensities for $\mathbf{E} \parallel c_R$ and $\mathbf{E} \perp c_R$, and $\rho_{d_\parallel}$ and ρ_{π^*} are the unoccupied densities of states of the $d_\parallel$ and π^* orbitals, respectively. Of particular importance are the changes in the spectral features in the excitonic part of the spectra for photon energies in the range from 512.5 to 516 eV that probe the valence electron states. This energy range is indicated by the dashed vertical lines in Fig. 2a,b. Over this energy range, the intensity difference ($I_\parallel - I_\perp$) is clearly more negative in the insulating state by comparison with the metallic state. This can be understood as arising from orbital polarization in the insulating state due to the selective filling of $d_\parallel$ orbitals; in the metallic state, on the other hand, the filling is isotropically distributed between the $d_\parallel$ and π^* orbitals (Fig. 1c,d). Consequently, the intensity difference at the first peak in the $I_\parallel - I_\perp$ curve[26] is approximately -0.55 (at ~514.3 eV) in the insulating state; by comparison this is ~0.1 (at ~514.1 eV) in the metallic state. The measured changes in the spectral features across the MIT agree very well with those previously reported[11] on single-crystalline bulk VO_2 and highlight the high quality of the thin-film samples
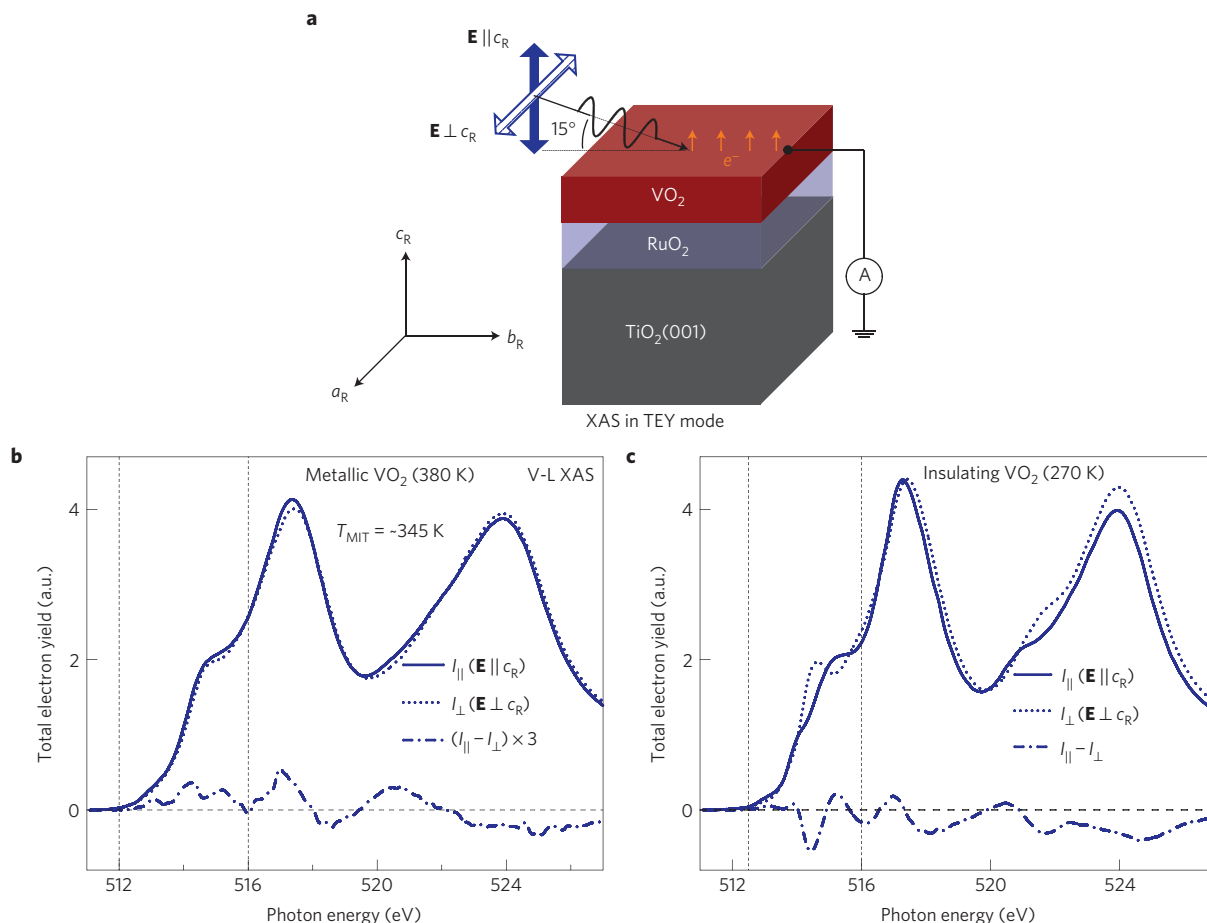
Figure 2 | Polarization-dependent XAS. a, Schematic of the XAS measurement geometry. The X-ray beam is incident at 15° to the sample surface and the photon polarization is either parallel ($\mathbf{E} \parallel c_R$) or perpendicular ($\mathbf{E} \perp c_R$) to c_R. The orange arrows represent the X-ray-excited electron current. **b,c**, Polarization-dependent. V L edge XAS spectra are shown in the metallic state (**b**) and the insulating state (**c**), for a VO$_2$ film with $T_{MIT} = \sim 345$ K. $I_\parallel$ and $I_\perp$ are the TEY intensities corresponding to $\mathbf{E} \parallel c_R$ and $\mathbf{E} \perp c_R$. The differences between these spectra are also shown. The vertical dashed lines indicate the approximate energy range of excitations into the vacant $d_\parallel$ and π^* electronic states.

used in this study, because the V $2p$ core-level binding energies are sensitive to the local atomic environment and the valence state of the vanadium ion[23,26,27]. More importantly, they validate our qualitative interpretation of the XAS data, which will form the basis for understanding the strain-dependent changes in orbital occupation discussed below.

In Fig. 3a, we plot $I_\parallel - I_\perp$ for three samples with different T_{MIT}. A comparison within the excitonic region of the spectra clearly shows that $I_\parallel - I_\perp$ increases with decreasing T_{MIT}. The sample with the smallest T_{MIT} has the largest apical V–O bond length (Fig. 1f) and consequently the smallest p–d overlap along the apical direction. This means that the energy of the π^* valence electronic states is lowered relative to that of the $d_\parallel$ valence states, thereby transferring electrons from the $d_\parallel$ to the π^* orbitals. The transfer of electrons between the valence orbitals is a direct consequence of charge conservation assuming that the V ion is in the $3d^1$ valence state for the three different strains. This transfer increases $\rho_{d_\parallel}$ and correspondingly decreases $\rho_{\pi*}$ that account for the increasingly positive $I_\parallel - I_\perp$ that we measure for decreasing T_{MIT}. In particular, $I_\parallel - I_\perp$ increases from 0.1 for the least strained sample (T_{MIT} of ~ 345 K) to 0.3 for the most strained sample (T_{MIT} of ~ 288 K). The magnitude of this strain-dependent change in $I_\parallel - I_\perp$ is almost one-third the change in $I_\parallel - I_\perp$ across the MIT for the sample with a T_{MIT} (~ 345 K) closest to that of bulk VO$_2$ (~ 340 K). This means that the strain-dependent orbital occupation changes in the metallic state are comparable in magnitude to the orbital occupation changes across the MIT.

In the insulating state, the π^* orbitals lie above E_F and a transfer of electrons is not expected for the relatively small changes in lattice parameters that we measure. This is in accord with the negligible changes in $I_\parallel - I_\perp$ that we find for the same three samples in the insulating state within the energy range of 512.5–516 eV (Fig. 3b). These changes in the relative orbital energies in the metallic and the insulating states are shown schematically in Fig. 3c,d, respectively. Remarkably, these results suggest that the metallic state's orbital occupation is directly related to T_{MIT}, while the insulating state's electronic distribution changes little.

To elucidate the role of orbital occupation in the MIT of VO$_2$, we compare in Fig. 4 the changes in dichroism and the magnitude of the structural changes across the transition to T_{MIT}. First, we find that the dichroic signal summed over the energy range from 512.5 to 516 eV, that is, $100(I_\parallel - I_\perp)/(I_\parallel + I_\perp)$, increases as the T_{MIT} is decreased. Positive dichroism is a consequence of increased $\rho_{d_\parallel}$ (unoccupied $d_\parallel$), as explained earlier, and thus correlates with a decrease in $d_\parallel$ orbital occupation. Second, we find that the magnitude of the structural change inferred from the change in the average out-of-plane lattice spacing across the MIT decreases with decreasing T_{MIT} (Supplementary Section S8). As the $d_\parallel$ orbitals participate in the dimerization of the V ions along c_R, we conclude that there is a correlation between a decrease in the occupancy of the $d_\parallel$ valence electron states and the magnitude of the structural change as T_{MIT} is varied.
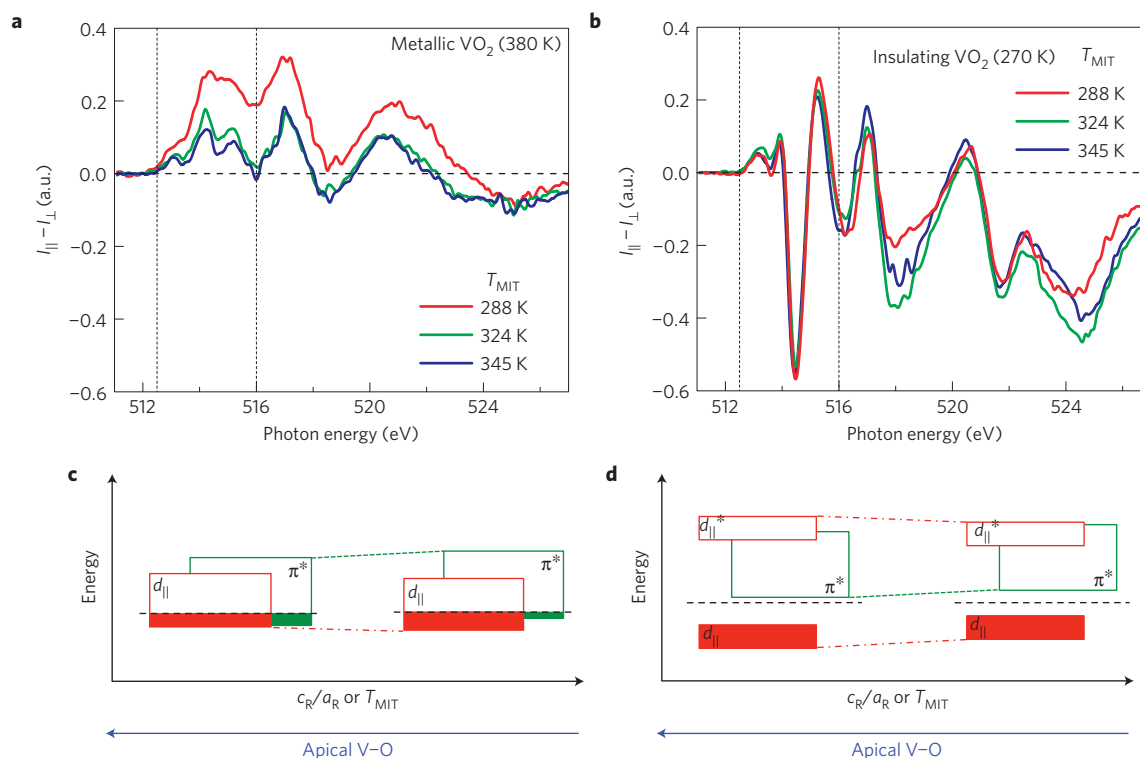
Figure 3 | Strain-dependent orbital-occupation changes. a,b, $I_\parallel - I_\perp$ in the metallic state (**a**) and the insulating state (**b**) for samples with various T_{MIT}. **c,d,** Schematic of changes in the valence electron states in the metallic state (**c**) and the insulating state (**d**) as T_{MIT} is changed.
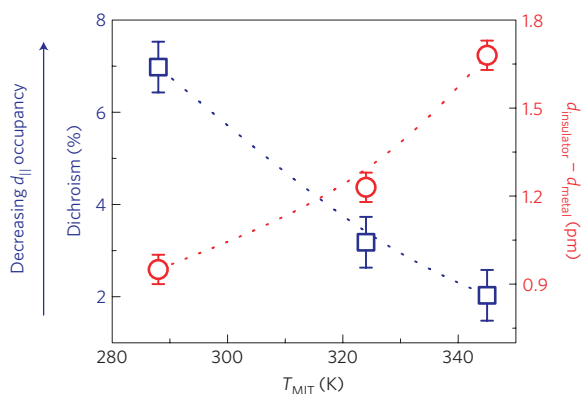
Figure 4 | Orbital–lattice correlation. Dichroism versus T_{MIT} in the metallic state for the three samples shown in Fig. 3. The dichroism is defined as $100(I_\parallel - I_\perp)/(I_\parallel + I_\perp)$ integrated over the energy range from 512.5 to 516 eV. A more positive dichroism corresponds to a lower T_{MIT} and a smaller $d_\parallel$ occupancy. The error bars correspond to the standard deviation in the dichroism measured for the three insulating state spectra in Fig. 3b, which are nominally identical in our model. Corresponding changes in the lattice are plotted on the right axis as the difference between the mean out-of-plane spacing of the $VO_2(001)$ film in the insulating ($d_{insulator}$) and the metallic (d_{metal}) states. The error bars correspond to measurement accuracy. $d_{insulator} - d_{metal}$ decreases with decreasing T_{MIT} and $d_\parallel$ occupancy, highlighting the significant role that the $d_\parallel$ orbital occupation plays in the MIT of VO_2. The dotted lines are a guide to the eye.

The electron–electron correlation energy[28] (U_{d-d}) could also influence T_{MIT}. However, this energy will be largest for the sample with the lowest T_{MIT} that has the largest apical V–O bond length and therefore the smallest bandwidth (the equatorial V–O bond length also changes but by only ~0.1% as shown in Fig. 1f). The presence of orbital-specific correlations can be ruled out

because it has been experimentally observed that both $d_\parallel$ and π^* bands have comparable bandwidths[16]. It therefore seems likely that orbital–lattice coupling plays a more significant role than U_{d-d} in determining T_{MIT} in VO_2. These conclusions are valid only when the bandwidth influences the Mott transition rather than changes in d band filling.

These experimental findings are clear evidence that the orbital occupancy in the metallic state of VO_2 sets the energy scale for the MIT. A similar orbitally driven Peierls state with tetramer ordering leading to a metal–insulator transition was suggested for compounds crystallizing in the spinel structure[29] and trimeron formation was experimentally shown in Fe_3O_4 (ref. 30). Both rutile and spinel compounds have edge-sharing octahedra that mediate metal–metal bonding[15] and the presence of a Peierls-like distortion along the metal–metal chains might very well suggest that they have a common origin. In addition, our findings open new ways to the orbital control of the MIT in VO_2, for example, by an interface-mediated orbital reconstruction[31] or by the formation of quantum wells[32]. Our experimental results should inspire further theoretical work on predicting the role of orbital filling and metal–metal bonding in triggering an MIT in VO_2 and other related materials.

Methods

Before thin-film deposition, 10 mm × 10 mm $TiO_2(001)$ substrates were pre-cleaned by ultrasonically soaking in deionized water for 20 min and etching for 60 s in ammonium fluoride (NH_4F)-buffered hydrofluoric acid (commercially available 7:1 buffered oxide etch from J. T. Baker). The substrates were then baked at 400 °C for 1 h in the deposition chamber. RuO_2 buffer layers were reactively sputtered from a metallic ruthenium target in a 3 mtorr Ar + O_2 gas mixture with ~8% oxygen. The substrates were maintained at a temperature of 300 °C during deposition. After RuO_2 deposition, the substrates were transferred *in situ* to a pulsed laser deposition system and VO_2 films were laser deposited in ~10 mtorr of O_2 with a laser energy density of ~1 J cm^{-2} operating at a pulse frequency of 2 Hz. Deposition was carried out at the optimal substrate temperatures of 400 °C for VO_2/TiO_2 and 300 °C in the case of $VO_2/RuO_2/TiO_2$ to minimize inter-diffusion at the VO_2 and RuO_2 interface. VO_2 films, ~30 nm thick, were deposited on RuO_2-buffered substrates

and ~10-nm-thick VO_2 films were deposited on substrates without the buffer layer (also see Supplementary Sections S4 and S6).

X-ray absorption and linear dichroism measurements were carried out at the undulator beamline 4.0.2 of the Advanced Light Source in TEY mode with an energy resolution of ~0.1 eV. The average probing depth for soft X-rays in TEY mode was estimated to be about 5 nm, thus providing a bulk-sensitive probe of the VO_2 films, and minimizing the effects from surface adsorbates. The X-ray measurement spot size in the normal incidence geometry was focused down to ~100-μm diameter. Each sample was characterized using nearly 100% horizontally or vertically polarized X-ray beams at an incidence angle of 15° as measured from the sample plane. In such a grazing measurement geometry the X-ray electric field is oriented parallel to the surface for vertically polarized light, and almost perpendicular to the surface for horizontally polarized light, thus providing maximum sensitivity to changes in orbital character along the different crystallographic axes. Cryogenic cooling with liquid nitrogen and conductive heating with a built-in heating element was used to control the sample temperature to within ±0.1 K. Measurements were carried out at several locations on each sample, to exclude the possibility of X-ray beam damage. Data collected in the TEY mode were normalized to the O K post-edge background intensity after the V L_3 pre-edge background intensity was set to zero.

X-ray diffraction measurements were performed on a Bruker D8 discover system with monochromatic Cu Kα radiation that gives ≤0.01° angular resolution. A variable-temperature stage with a tungsten-heating element and cryogenic cooling by liquid nitrogen was used to control the sample temperature to within ±0.5 K. The stage was fitted with a beryllium window that is largely transparent to X-rays. Samples were maintained at the measurement temperature for at least 15 min before data acquisition. Electrical transport measurements were performed in a Quantum Design DynaCool cryostat in the four-point measurement geometry. Electrical connections to the VO_2 films were made by ultrasonically wire-bonded aluminium contacts. Resistance of the samples was continuously measured during continuous cooling or warming at a rate of 5 K min^{-1}.

References

1. Imada, M., Fujimori, A. & Tokura, Y. Metal–insulator transitions. *Rev. Mod. Phys.* **70,** 1039–1263 (1998).
2. Bednorz, J. G. & Müller, K. A. Possible high T_c superconductivity in the Ba–La–Cu–O system. *Zeit. Für. Phys.* **64,** 189–193 (1986).
3. Torrance, J. B., Lacorre, P., Asavaroengchai, C. & Metzger, R. M. Why are some oxides metallic, while most are insulating? *Physica C* **182,** 351–364 (1991).
4. Bocquet, A. E., Saitoh, T., Mizokawa, T. & Fujimori, A. Systematics in the electronic structure of 3d transition-metal compounds. *Solid State Commun.* **83,** 11–15 (1992).
5. Jin, S. *et al.* Thousandfold change in resistivity in magnetoresistive La–Ca–Mn–O films. *Science* **264,** 413–415 (1994).
6. Tokura, Y. & Nagaosa, N. Orbital physics in transition-metal oxides. *Science* **288,** 462–468 (2000).
7. Zeches, R. J. *et al.* A strain-driven morphotropic phase boundary in $BiFeO_3$. *Science* **326,** 977–980 (2009).
8. Morin, F. J. Oxides which show a metal-to-insulator transition at the Néel temperature. *Phys. Rev. Lett.* **3,** 34–36 (1959).
9. Abbate, M. *et al.* Soft-x-ray-absorption studies of the electronic-structure changes through the VO_2 phase transition. *Phys. Rev. B* **43,** 7263–7266 (1991).
10. Biermann, S., Poteryaev, A., Lichtenstein, A. I. & Georges, A. Dynamical singlets and correlation-assisted Peierls transition in VO_2. *Phys. Rev. Lett.* **94,** 026404 (2005).
11. Haverkort, M. W. *et al.* Orbital-assisted metal-insulator transition in VO_2. *Phys. Rev. Lett.* **95,** 196404 (2005).
12. McWhan, D. B., Marezio, M., Remeika, J. P. & Dernier, P. D. X-ray diffraction study of metallic VO_2. *Phys. Rev. B* **10,** 490–495 (1974).
13. Eyert, V. The metal-insulator transitions of VO_2: A band theoretical approach. *Ann. Phys.* **11,** 650–704 (2002).
14. Goodenough, J. B. The two components of the crystallographic transition in VO_2. *J. Solid State. Chem.* **3,** 490–500 (1971).
15. Goodenough, J. B. Direct cation–cation interactions in several oxides. *Phys. Rev.* **117,** 1442–1451 (1960).
16. Koethe, T. C. *et al.* Transfer of spectral weight and symmetry across the metal–insulator transition in VO_2. *Phys. Rev. Lett.* **97,** 116402 (2006).
17. Tanaka, A. On the metal–insulator transitions in VO_2 and Ti_2O_3 from a unified viewpoint. *J. Phys. Soc. Jpn* **73,** 152–162 (2004).
18. Butler, S. R. & Gillson, J. L. Crystal growth, electrical resistivity and lattice parameters of RuO_2 and IrO_2. *Mater. Res. Bull.* **6,** 81–89 (1971).
19. Grant, F. A. Properties of rutile (titanium dioxide). *Rev. Mod. Phys.* **31,** 646–674 (1959).
20. Muraoka, Y., Ueda, Y. & Hiroi, Z. Large modification of the metal–insulator transition temperature in strained VO_2 films grown on TiO_2 substrates. *J. Phys. Chem. Solids* **63,** 965–967 (2002).
21. Pouget, J. P., Launois, H., D'Haenens, J. P., Merenda, P. & Rice, T. M. Electron localization induced by uniaxial stress in pure VO_2. *Phys. Rev. Lett.* **35,** 873–875 (1975).
22. Ferrari, C., Buffagni, E. & Rossi, F. in *Characterization of Semiconductor Heterostructures and Nanostructures* (eds Agostini, G. & Lamberti, C.) Ch. 3 (Elsevier, 2013).
23. De Groot, F. M. F. X-ray absorption and dichroism of transition metals and their compounds. *J. Electron Spectrosc. Relat. Phenom.* **67,** 529–622 (1994).
24. De Groot, F. M. F. Oxygen 1s X-ray-absorption edges of transition-metal oxides. *Phys. Rev. B* **40,** 5715–5723 (1989).
25. De Groot, F. High-resolution X-ray emission and X-ray absorption spectroscopy. *Chem. Rev.* **101,** 1779–1808 (2001).
26. Park, J. H. *et al.* Spin and orbital occupation and phase transitions in V_2O_3. *Phys. Rev. B* **61,** 11506–11509 (2000).
27. Sawatzky, G. A. & Post, D. X-ray photoelectron and Auger spectroscopy study of some vanadium oxides. *Phys. Rev. B* **20,** 1546–1555 (1979).
28. Zaanen, J., Sawatzky, G. A. & Allen, J. W. Band gaps and electronic structure of transition-metal oxides. *Phys. Rev. Lett.* **55,** 418–421 (1985).
29. Khomskii, D. I. & Mizokawa, T. Orbitally induced Peierls state in spinels. *Phys. Rev. Lett.* **94,** 156402 (2005).
30. Senn, M. S., Wright, J. P. & Attfield, J. P. Charge order and three-site distortions in the Verwey structure of magnetite. *Nature* **481,** 173–176 (2012).
31. Chakhalian, J. *et al.* Orbital reconstruction and covalent bonding at an oxide interface. *Science* **318,** 1114–1117 (2007).
32. Pardo, V. & Pickett, W. E. Half-metallic semi-Dirac point generated by quantum confinement in TiO_2/VO_2 nanostructures. *Phys. Rev. Lett.* **102,** 166803 (2009).

Acknowledgements

Author contributions

N.B.A., M.G.S. and S.S.P.P. designed the study. N.B.A. deposited VO_2 films and L.G. deposited RuO_2 films. X-ray diffraction and electrical transport measurements were performed and analysed by N.B.A., M.D. and M.C. with help from L.G. A.X.G., N.B.A., A.H.R., R.K. and H.O. carried out and analysed the X-ray absorption measurements, with assistance from C.A.J. and E.A. and under the supervision of H.A.D. M.G.S. helped with X-ray absorption data analysis and along with K.P.R. provided thin-film deposition expertise. N.B.A. and S.S.P.P. wrote the paper with contributions from A.X.G., H.A.D. and M.G.S. All authors discussed the results and commented on the manuscript.

Additional information

Competing financial interests

The authors declare no competing financial interests.